PAPER • **OPEN ACCESS**

Efficiency of automotive electric supercharging compressors

To cite this article: Pierre Podevin *et al* 2020 *IOP Conf. Ser.: Mater. Sci. Eng.* **1002** 012032

Efficiency of automotive electric supercharging compressors

Pierre Podevin[1,6], Christelle Périlhon[1], Michael Deligant[2], Plamen Punov[3], Adrian Clenci[4] and Guillaume De La Bourdonnaye[5]

[1] Laboratoire LIFSE, Le Cnam, Conservatoire national des arts et métiers, 75003 Paris, France
[2] Laboratoire LIFSE, Arts et Métiers ParisTech, 75013 Paris, France
[3] Department of Combustion Engines, Automobile Engineering and Transport, Technical University – Sofia, 1756 Sofia, Bulgaria
[4] Department Automobiles and Transport, University of Pitesti, 110040 Pitesti, Romania
[5] Air charging system, Valeo, 95892 Cergy Pontoise, France

[6] Email: pierre.podevin@lecnam.net

Abstract. The automotive electric supercharger provides high torque at low engine speeds. During accelerations, it fills the power gap due to the turbocharger's inertia and avoids turbo lag. Its operation is of short duration because once this deficit has been juggled, it must be stopped in order not to generate unnecessary electricity consumption and to avoid overheating of the electric motor which would compromise its lifetime. Usually the power of automotive turbocharger is calculated assuming an adiabatic air compression and the adiabatic efficiency is assessed. At low speed or for low compression ratio, which is the case of electric supercharger, this hypothesis is no more valid and special experiments have to be done. On our test bench the compressor is driven by a turbine supplied with cold compressed air. Between the compressor and the turbine, a torque meter is inserted to measure the power given to the compressor shaft. The tests were conducted with a non-insulated compressor and an insulated compressor for eight iso-speeds. Additional tests were carried out to assess the actual power supplied to the fluid including bearing losses measurements and to assess the influence of different preload springs used to counter the axial thrust of the compressor. This article presents and analyses the results of this work.

1. Introduction

The automobile transport is responsible to a significant part of greenhouse gases due to burning the fossil fuels in internal combustion engines. In order to reduce global warming, European commission imposed a new CO_2 emissions target for passenger cars that will be fully applied in 2021. The new reference target value was set to 95 g/km which means reduction by 27% compared to previous legislation [1]. Moreover, more restrictive targets were defined for 2025 and 2030 that account to 15% and 37.5% CO_2 reduction compared to 2021. Based on the real vehicle CO_2 emissions, it is obviously that in long term a significant number of zero and low emission vehicle need to be in the fleet. However, in short term the main energy source will still remain the internal combustion engine with rising level of electrification and hybridization [2]. In order to increase the engine thermal efficiency turbocharging technology has been applied for many years both in diesel and gasoline engines. However, turbochargers cannot meet all the engine requirements, especially the engine performance at low speed and transient operating model. That could be overcome by applying modern technics such as: variable geometry turbine, dual stage turbocharging (widely used in diesel engines), twin scroll turbines or using additional compressor [3-5]. This additional compressor could be mechanically driven or electrically assisted. Electrically assisted supercharger could be adapted to nominal voltage within the range of 12 V to 48 V [6], thus it can be applied to mild-hybrid passenger cars as well. Usually, it operates for limited time (less than 20 s) during acceleration phase at low engine speed and full load. Therefore, it offers better engine acceleration at low speed in combination with high torque and lower fuel consumption up to 25% [7].

In order to evaluate overall engine efficiency, the electrical consumption of the additional supercharger has to be taken into accounts. This consumption is related to operation strategy, mechanical losses, motor efficiency and compressor efficiency. The most significant losses are aerodynamic, thermal and mechanical losses within the compressor. A literature review shows that the performance of this type of electric supercharger is not covered in publications. For that reason, this article aims to study the isentropic efficiency on an electrically assisted supercharger based on experimental test. The tests were conducted at different operating conditions as the effect of insulation and bearings loads was evaluated. The efficiency was evaluated based on thermodynamic parameters and compressor power balance.

2. Mathematical background

The power and efficiency of a turbomachine can be expressed according to the first law of thermodynamics. Applied to a compressor between inlet point 1 and outlet point 2, for a steady-state flow and neglecting the potential energy, the internal work W_i is [8]:

$$W_i = (h_{i2} - h_{i1}) - Q, \tag{1}$$

where W_i is internal work on the compressor wheel; h_i – stagnation enthalpy; Q – heat exchanged with the external environment; $Q < 0$ if the heat is transferred to the outside; $Q > 0$ if the heat is received from the outside; $Q = 0$ for an adiabatic evolution.

It should be noted that the internal work W_i on the transmission shaft is the work received by the compressor wheel in contact with the fluid. It is therefore equal to the work of the mobile channels added to that absorbed by disk friction [8]:

$$W_i = W_{ch} + W_{frd}, \tag{2}$$

where W_{ch} is impeller channel work; W_{frd} – disk friction work.

This internal work is also equal to the work on the shaft measured by a torque meter, reduced by the work absorbed by the bearings:

$$W_i = W_{shaft} - W_{frb}, \tag{3}$$

where W_{shaft} is work on the shaft measured by the torquemeter; W_{frb} – work of the bearing system.

In the case of an adiabatic machine, the work for a perfect ideal gas is thus simply written:

$$W_{adia} = h_{i2} - h_{i1} = c_p(T_{i2} - T_{i1}), \tag{4}$$

where T_i is stagnation temperature; c_p – specific heat at constant pressure.

This work is then "easily" determined by measuring the two inlet and outlet temperatures and isentropic efficiency is:

$$\eta_{is} = \frac{W_{is}}{W_{adia}} = \frac{T_{i2is} - T_{i1}}{T_{i2} - T_{i1}}, \tag{5}$$

where T_{i2is} is stagnation temperature of the isentropic theoretical evolution obtained by:

$$T_{i2is} = T_{i1} \left[\frac{p_{i2}}{p_{i1}}\right]^{\frac{\gamma-1}{\gamma}}, \tag{6}$$

where p_i is stagnation pressure.

In fact, while the adiabatic assumption can be used for large turbomachines, the operation of small turbomachines diverges from it at low speeds and low loads. Particularly on test benches with a turbine supplied with hot gas, heat transfers are established from the turbine to the colder compressor through mechanical components and lubricating oil. Many studies have been done to estimate heat exchange [9-11]. If Q is known, calculation of W_i according to equation (1) does not present major difficulties.

Another way to determine the internal work, is to measure W_{shaft} the mechanical work on the shaft using a torque meter and to determine the mechanical losses W_{frb} of the bearings. Then W_{i} is calculated from equation (3). Calculations of mechanical losses are presented in various papers [12-15].

In our laboratory, we have used a special torque meter to measure directly the mechanical work and done some experiments to determine the mechanical losses presented in this paper.

3. Test bench overview

The compressor is a prototype electric compressor developed by Valeo. It is driven by an 48V electric motor. It reduces turbocharger turbo lag and provides high torque at low engine speeds. Its design and purpose make it necessary for its operation to be intermittent. Also, the electric motor could not be used for our experiments.

To assess the torque transmitted to the compressor, we have used a special torquemeter able to run at 120000 rpm, the maximum speed of the compressor being 80000 rpm. The torque is measured with an accuracy of ±0.00021 Nm. Compressor speed and torque values are given by the torquemeter. This torquemeter is placed between the compressor and a turbine. The turbine acts as the electric motor for the compressor with the benefit of being able to operate continuously at a given operating point.

The turbine is fed by dry compressed air close to ambient temperature, which avoids hot gas supply problems but requires a large air compression and drying plant. A schematic of the test bench is given in figure 1. A specific assembly was set up in order to mount it on our bench, figure 2. The bearings and the preload spring were kept.

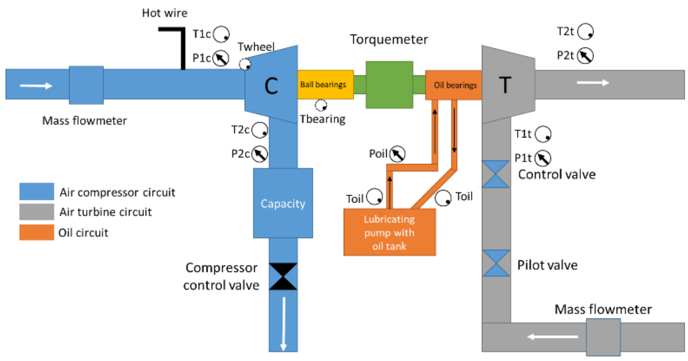

Figure 1. Schematic of the test bench.

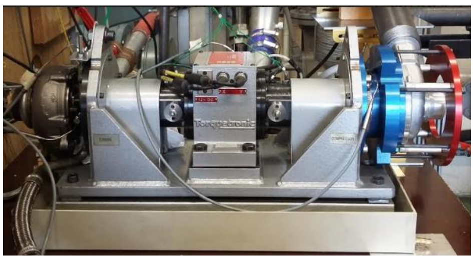

Figure 2. Compressor Assembly.

The usual measurements were made, i.e. temperatures and pressures at the compressor inlet and outlet; the air flow rate was measured by a thermal mass flow meter. The temperatures were measured with platinum resistance thermometers PT100 and pressure with piezoresistive sensors. Additional measurements were made on the turbine side.

A capacity was fitted on the circuit to increase the surge phenomenon. The definition of the surge line and appearance of surge was presented in [16-17].

All the signals are converted into voltage in the range 0-10 V and sent to a data acquisition card. The data are visualized and acquired using a LabVIEW program. All the data are recorded in a file and processed in an Excel file.

4. Experimental results

The compressor characteristic curves are expressed as iso-speed values.

Since the measured temperature is not really the stagnation temperature, a α correction is applied to the measurement to calculate it in accordance with usual practice in our laboratory.

$$T_m = T_s + \alpha \frac{V^2}{2Cp}, \tag{7}$$

$$T_i = T_s + \frac{V^2}{2Cp}, \tag{8}$$

where T_m is measured temperature; T_s – static temperature; v – air flow speed.

The stagnation pressures are calculated from the static pressures measured assuming a reversible adiabatic evolution.

$$\frac{p_i}{p_s} = \left(\frac{T_i}{T_s}\right)^{\frac{\gamma}{\gamma-1}}. \tag{9}$$

The pressure ratio is:

$$Pr = \frac{p_{i2}}{p_{i1}}. \tag{10}$$

Characteristic curves represent stagnation Pressure ratio versus Air flow rate. Air flow and speed are corrected according to the following reference values: $T_{ref} = 298$ K, $p_{ref} = 100$ kPa.

According to equation (1), the internal compressor power, P_i is:

$$P_i = \dot{m}_a Cp(T_{i2} - T_{i1}) - \dot{Q}, \tag{11}$$

where $\dot{m}_a$ is air flow rate, which can also be written:

$$P_i = P_{enth} - \dot{Q}, \tag{12}$$

where P_{enth} being the enthalpic power:

$$P_{enth} = \dot{m}_a \, Cp(T_{i2} - T_{i1}). \tag{13}$$

This enthalpic power is equal to adiabatic power P_{adiab} for an adiabatic compression or if heat exchange can be neglected. Isentropic efficiency is calculated according to equation (5).

4.1. Isentropic efficiency evaluation with and without insulation

Measurements are made by steps of 5000 rpm from 30000 to 75000 rpm. Particular attention has been paid to the temperature stabilization. The isentropic efficiency is displayed directly on the computer control screen. When it is stabilized to within 1%, the point is recorded. This takes approximately 20 min for the first point (compressor outlet vane fully open) and then about 5 min for the following points.

First measurements were done without insulation, see figure 2. Then to reach adiabatic conditions mineral wool was wrapped all around the compressor figure 3.

Figure 3. Insulation of the compressor.

Figure 4 shows the results of pressure ratio versus Air flow rate and figure 5 Isentropic efficiency versus air flowrate with and without insulation. For reasons of clarity, 3 speed lines are shown.

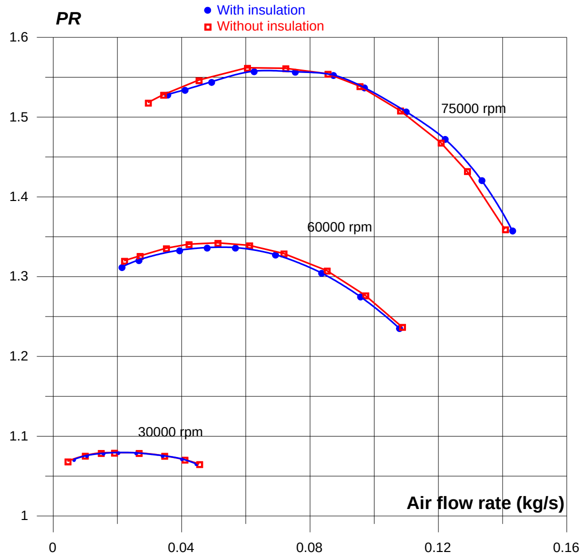

Figure 4. Comparison of pressure ratio vs air flow rate with and without insulation.

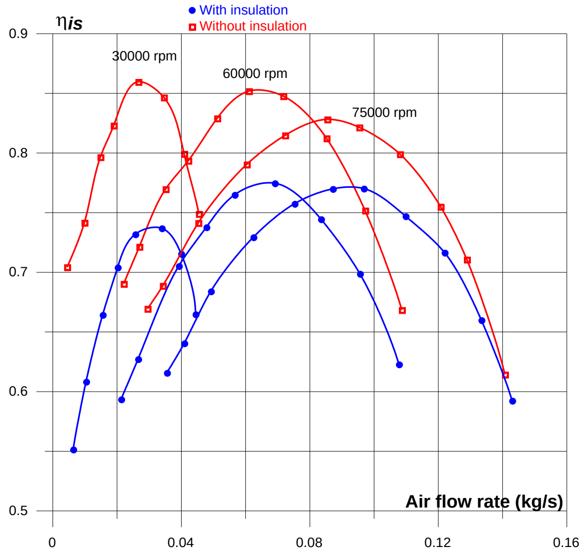

Figure 5. Comparison of isentropic efficiency vs air flow rate with and without insulation.

Insulation has no effect on the characteristic curve of pressure ratio vs air flow rate. The efficiency values with insulation are now in the range of 75 to 77%, maximum expected values from Valeo calculations.

By subtracting the enthalpic power before and after insulation, the heat losses during the initial setup can be estimated, figure 6.

Heat losses at low speeds are obviously lower than at high speeds, but due to a lower power delivery they have a much greater impact on the calculation of isentropic efficiency.

During the 75000 rpm test with insulation, a temperature reading of the surfaces was carried out with an infrared thermometer. It appears that the compressor is not completely isolated and that a small heat exchange still takes place with the frame of the torque meter. During this reading, the compressor outlet temperature was T_{2m} = 78°C and the temperature of the torquemeter bearings varied from 38 to 40°C, figure 9.

IOP Conf. Series: Materials Science and Engineering 1002 (2020) 012032 doi:10.1088/1757-899X/1002/1/012032

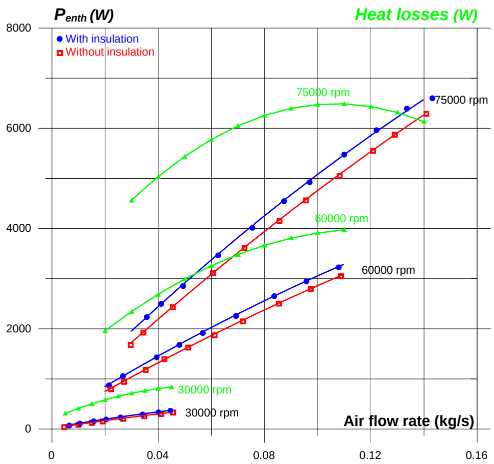

Figure 6. Comparison of heat losses vs air flow rate with and without insulation.

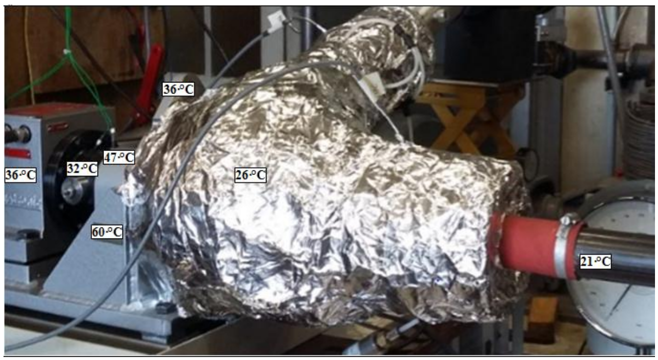

Figure 7. Measurements of the surface temperatures.

As it seemed difficult to provide better insulation, we conducted a test to observe the influence of insulation around the bearings by removing this insulation.

Temperature around the bearings reaches 80°C, figure 8, and the effect of this insulation on isentropic efficiency can be clearly seen, figure 9. Less insulation causes an artificial increase in isentropic efficiency.

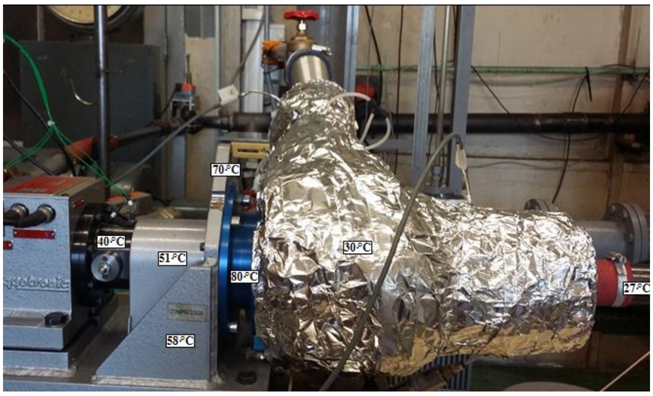

Figure 8. Measurements of the surface temperatures without insulation of the bearings.

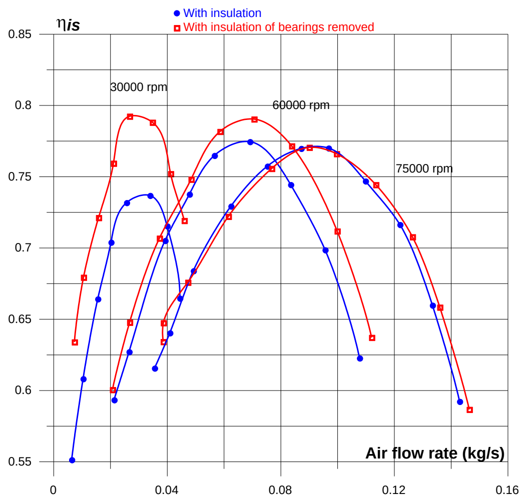

Figure 9. Isentropic efficiency vs air flow rate with and without insulation of the bearings.

From these experiments it appears that heat exchange cannot be totally avoided. We therefore tried to calculate the real power given to the air flow, considering the torque measured by the torquemeter.

4.2. Evaluation of shaft power with full insulation

The use of a torquemeter makes it possible to measure the real power given to the compressor shaft.

Here we considered the tests with full insulation. A comparison of the mechanical power measured by the torquemeter P_{shaft} and the compressor power P_{enth} is plotted in figure 10. The shaft power, P_{shaft} is obviously greater than the adiabatic compressor power P_{enth}. At high speed, i.e. 75000 rpm, there is a maximum gap of around 400 W. At medium speed, 60000 rpm, the medium difference is about 200

W. At 30000 rpm, the difference cannot be clearly seen in this figure. A zoom in at 30000 rpm figure 11 shows that P_{shaft}, is always greater than P_{enth}.

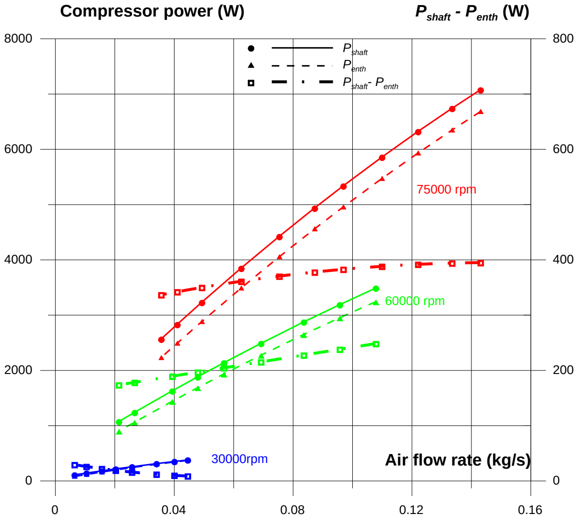

Figure 10. Comparison of insulated compressor enthalpic power and shaft power vs air flow rate.

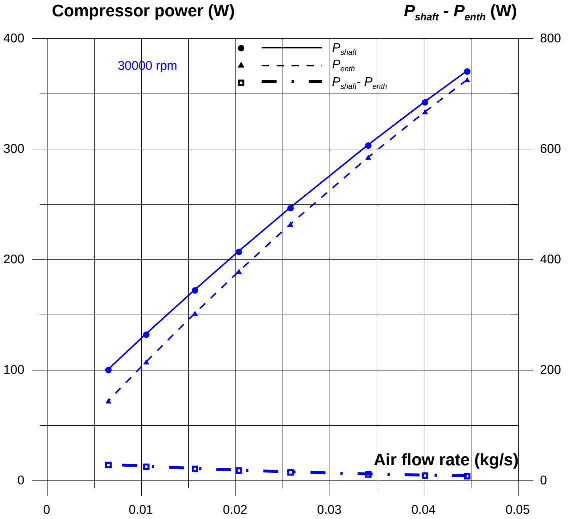

Figure 11. Comparison of insulated compressor enthalpic power and shaft power vs air flow rate (zoom).

However, it seems very difficult to measure the adiabatic power of the compressor P_{enth} accurately in this operating area due to a very low temperature rise between the compressor inlet and outlet. This temperature rise at the maximum flow rate is 8.1°C and 10.6°C at the minimum flow rate.

To determine the real internal power given to the fluid P_i, it is necessary to know the bearing friction losses P_{frb}. The internal power being equal to the power given to the shaft P_{shaft} minus the power due to bearing friction losses P_{frb}, equation (3) becomes:

$$P_i = P_{shaft} - P_{frb}. \tag{14}$$

To estimate these bearing losses, we performed the experiments detailed below.

4.3. Bearing friction losses

A new rotating assembly with a spacer instead of the wheel was supplied by Valeo figure 12.

The bearings were new. After running for 15 minutes at 30000 rpm, the torque decreased from 0.045 Nm (140 W) to 0.015 Nm (47 W). Nevertheless, this running-in period was insufficient, and a minimum friction power of 9 W was later obtained for 30000 rpm.

As bearing friction may be impacted by axial loads, measurements were performed varying axial load. The first experiment was conducted with the original spring and then a washer was added to increase the preload. Then Valeo provided us with several springs of different stiffnesses.

In real operating conditions, the aerodynamic gas load is estimated to be between 10 to 60 N by Valeo. Spring stiffnesses were measured on the pulling machine in Valeo's Cergy metrology laboratory.

At low load, the effect of spring stiffness can be clearly observed on the torque curves in figure 13. We measured the torque at 30000 rpm then up to 80000 rpm by steps of 10000 rpm. The speed was then decreased with the same step. Some hysteresis can be seen.

Figure 12. Rotor assembly with the wheel replaced by a spacer.

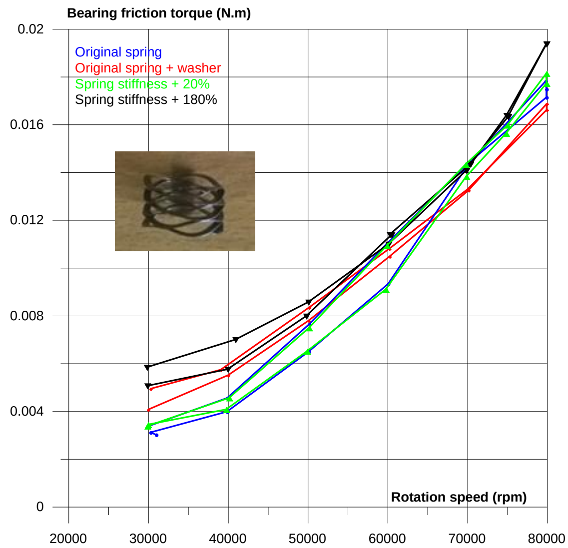

Figure 13. Bearing friction for different spring loads and rotation speeds.

As the axial thrust at low speed is weak, it appears necessary to choose the spring suited to the maximum load and not to oversize it in order to reduce friction losses at low speed.

Figure 14 plots friction power versus rotation speed for the original spring and for the spring with maximum stiffness. The friction of the original spring can be estimated by a power law. This law was later applied to calculate internal power.

The last experiments on bearing friction aimed to see the influence of temperature on bearing losses. Hot air was introduced by a heat gun at the outlet of the volute, to increase the temperature of the body which maintains the bearings from 30 to 80°C. The reduction in friction losses was relatively small, about 10 W at 75000 rpm, figure 15.

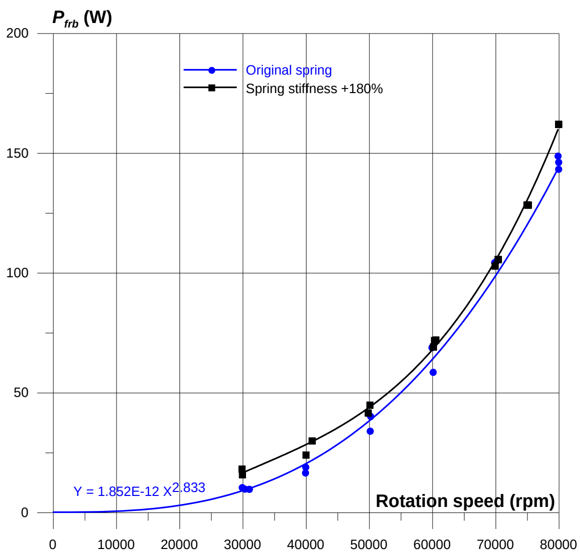

Figure 14. Bearing friction for different spring loads vs rotation speeds.

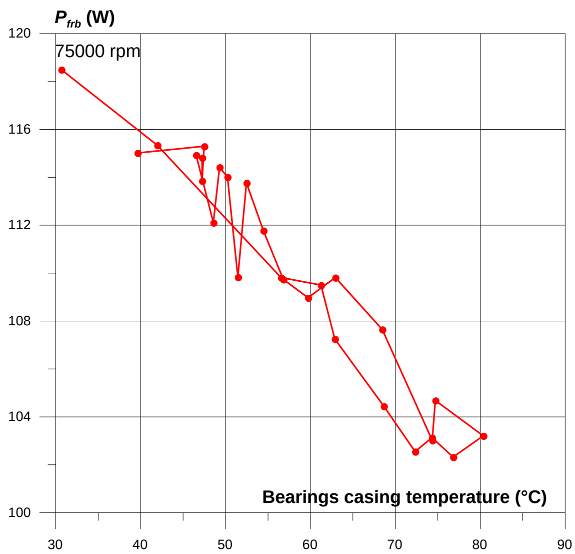

Figure 15. Variation of bearing friction power in the case of heated body at 75000 rpm.

4.4. Analysis of the results

From the previous tests, it is possible to calculate the internal power P_i supplied to the fluid according to equation (14). The mechanical power is measured by the torquemeter and the bearing friction loss power P_{frb} calculated from the proposed power law figure 14. According to equations (12) and (14) thermal losses $\dot{Q}$ in this insulated case are given by:

$$\dot{Q} = P_{enth} - P_{shaft} + P_{frb}. \tag{15}$$

In figure 16, we added the speed 50000 rpm to observe the evolution of these thermal losses more closely. As Q is negative, which means that heat is transferred from the fluid to the ambient, on the figure $-\dot{Q}$ is represented.

For 60000 and 75000 rpm, the thermal losses increase with the flow rate, are almost constant at 50000 rpm and decrease at 30000 rpm. It should be noted that at 30000 rpm there are negative losses ($-Q<0$), which means that the fluid receives heat from bearing power losses.

As a first approximation by averaging the thermal losses $-\dot{Q}$, it is possible to express this as a function of the compressor rotation speed and compare these against the friction losses figure 17.

As a result, despite the care taken with the insulation, the thermal losses are significant.

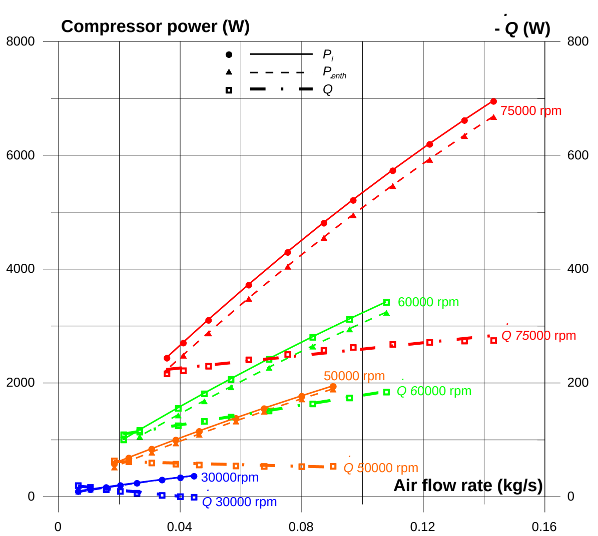

Figure 16. Insulated compressor power and thermal losses vs air flow rate.

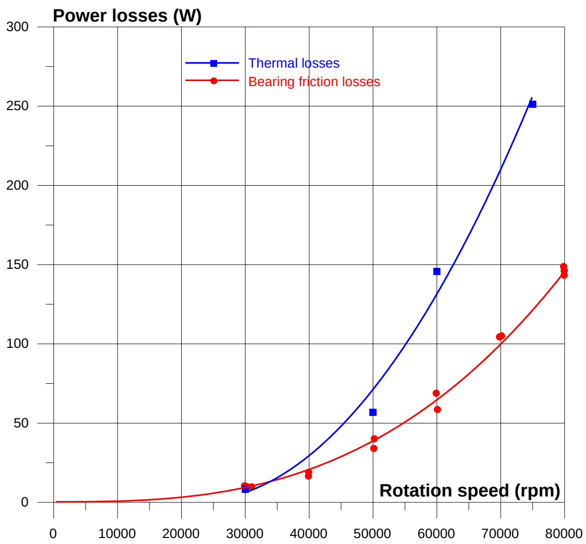

Figure 17. Friction and thermal losses for the insulated compressor vs rotation speed.

From equation (14), the power measured by the torquemeter and the proposed bearing friction power law figure 16 it is possible to calculate the internal power P_i supplied to the fluid and thus compare the isentropic efficiencies calculated from this power (16) with results obtained directly by measuring temperatures with the insulated compressor (5), see figure 18.

$$\eta_{is} = \frac{P_{is}}{P_i} = \frac{P_{is}}{P_{shaft} - P_{frb}} = \frac{\dot{m}_a c_p (T_{i2is} - T_{i1})}{P_i}. \tag{16}$$

As the calculated internal power is higher than the adiabatic power, the result is a decrease in efficiency for results obtained from the torquemeter rather than temperatures. This is expected as, even when insulated, the compressor is not adiabatic and because thermal losses are not taken into account in the efficiency calculated by equation (5).

The maximum isentropic efficiency of the compressor decreases from 77.5 to 72.5%. The maximum efficiency is practically constant for each iso-speed.

From the test results, the mechanical efficiency η_m can be plotted, figure 19, P_i being calculated with equation (14).

$$\eta_m = \frac{Pi}{Pshaft}. \tag{17}$$

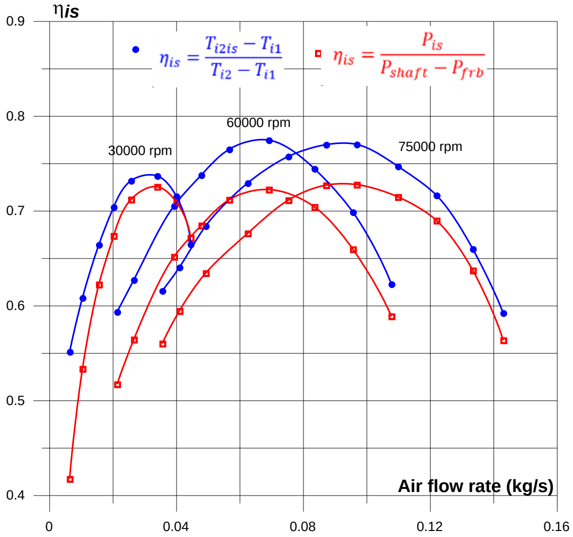

Figure 18. Isentropic efficiency vs air flow rate.

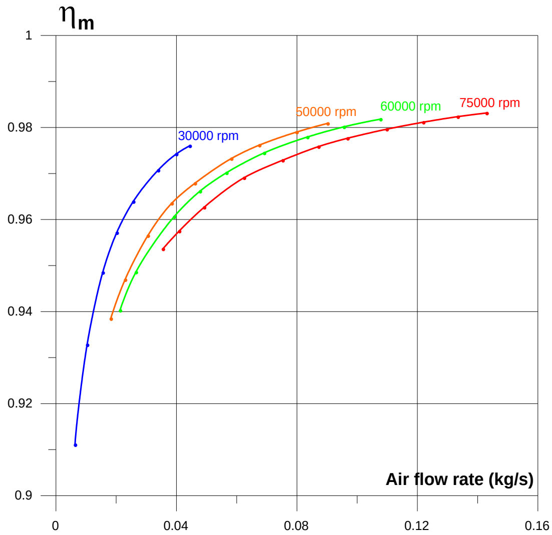

Figure 19. Mechanical efficiency vs air flow rate.

5. Conclusion

The tests revealed the influence of insulation on the performance measurement of the compressor. While the insulation has no influence on the Pressure ratio-Air flow rate characteristic curves, it does have an influence on the power transmitted from the compressor shaft.

If during compression a quantity of heat is exchanged with the outside environment, the power required for compression decreases. As a result, the compressor efficiency is improved.

However, if the measurement of compressor power is deduced from the first law of thermodynamics by considering the flow as adiabatic, the increase in isentropic efficiency calculated in this way is unrealistic.

By using ball bearings instead of oil bearings, it was hoped to encounter fewer difficulties in determining the actual performance of the compressor.

This is true for the determination of bearing losses. It has been shown that these are not very sensitive to axial thrust and therefore it is possible to calculate the internal power supplied to the fluid relatively easily.

As far as heat loss is concerned, simple insulation with mineral wool does not eliminate heat exchange. Some of the compression heat is transmitted by conduction to the compressor body and then to the torquemeter frame. At low engine speeds it is likely that it is the heat from friction losses of the bearings that is transmitted to the compressor.

It would therefore be advisable to ensure the connection of the compressor torquemeter with an insulating material in order to reduce thermal losses and possibly control the temperature of the bearings by a hydraulic circuit.

When considering the motorization of the compressor, what is important to know is the power that must be supplied to the compressor (not insulated). This is what the direct measurement with the torquemeter allows. However, this information is not sufficient. It is also necessary to ascertain that the compressor is adapted to its task by the adequacy of its operation with the demands required by the powertrain.

To be able to assess the efficacy of this machine, its efficiency is a perfectly adequate variable. Isentropic efficiency, why not? Polytropic or isothermal efficiency why not? All the powers of these theoretical evolutions are easy to calculate. However, the main problem remains to easily determine (without a torquemeter) the internal power when heat exchanges with the external environment cannot be neglected.

Acknowledgements
We would like to thank Valeo for funding this study and allowing us to use this compressor for further surge studies. We also thank the BTS Arras and BTS La Joliverie trainees as well as the engineering students of Cnam who made it possible to carry out these experiments successfully. The study was conducted within the frame of project "Amélioration de l'efficacité énergétique des véhicules routiers par optimisation du couplage moteur-turbocompresseur" funded by joint research program AUF-FRS 2018 (КП-06-Франкофония/3).

References
[1] European Commission. CO2 emission performance standards for cars and vans (2020 onwards) https://ec.europa.eu/clima/policies/transport/vehicles/regulation_en
[2] Ajanovic A and Haas R 2017 The impact of energy policies in scenarios on GHG emission reduction in passenger car mobility in the EU-15 *Renewable and Sustainable Energy Reviews* **68**(2) pp 1088–96
[3] Feneley A J, Pesiridis A and Andwari A M 2017 Variable Geometry Turbocharger Technologies for Exhaust Energy Recovery and Boosting-A Review *Renewable and Sustainable Energy Reviews* **71** pp 959–75
[4] Romagnoli A, Vorraro G, Rajoo S, Copeland C and Martinez-Botas R 2017 Characterization of a supercharger as boosting & turbo-expansion device in sequential multi-stage systems *Energy Conversion and Management* **136** pp 127–41
[5] Zi D, Zhang L, Chen B and Zhang Q 2019 Study of the electric-booster and turbo-generator system and its influence on a 1.5 L gasoline engine *Applied Thermal Engineering* **162** 114236
[6] Tran H H, Richard B, Gray K and Hall J M 2016 Developing a performance specification for an electric supercharger to satisfy a range of downsized gasoline engine applications *SAE Technical Paper*
[7] Baek S, Woo S, Kim Y and Lee K 2019 Prediction of turbocharged diesel engine performance equipped with an electric supercharger using 1D simulation *Energy* **185** pp 213–28
[8] Pluviose M and Périlhon C 2017 Turbomachines - Description et principes de base *Techniques de l'ingénieur* BM4280(2017)**v2** pp 1–17
[9] Bohn D, Heuer T and Kusterer K 2003 Conjugate flow and heat transfer investigation of a turbocharger, part 1: numerical results *Proc. of Turbo Expo 2003 (Atlanta, Georgia, USA)* Paper GT2003-38445 pp 715–22
[10] Baines N, Wygant K D and Dris A 2010 The Analysis of Heat Transfer in Automotive Turbochargers *Journal of Engineering for Gas Turbines & Power* **132**(4) 042301
[11] Chesse P, Chalet D and Tauxia X 2011 Impact of the heat transfer on the performance calculations of automotive turbocharger compressor *Oil & Gas Science and Technology - Revue d'IFP Energies nouvelles* **66**(5) pp 791–800
[12] Brouwer M D, Sadeghi F, Lancaster C, Archer J and Donaldson J 2013 Whirl and Friction Characteristics of High Speed Floating Ring and Ball Bearing Turbochargers *J. Tribol.* **135**(4) 041102
[13] Ashtekar A and Sadeghi F 2011 Experimental and Analytical Investigation of High Speed Turbocharger Ball Bearings *J. Eng. Gas Turbines Power* **133**(12) 122501
[14] Lamquin T and Gjika K 2009 Power losses identification on turbocharger hydrodynamic bearing systems: test and prediction *Proc. of ASME Turbo Expo (Orlando, Florida, USA)* GT2009-59599 pp 153–62
[15] Vanhaelst R, Kheir A and Czajka J 2016 A systematic analysis of the friction losses on bearings of modern turbocharger *Combustion Engines* **164**(1) pp 22–31
[16] Deligant M, Danlos A, Podevin P, Clenci A and Guilain S 2017 Surge detection on an automotive turbocharger during transient phases *IOP Conf. Ser.: Mater. Sci. Eng.* **52** 012082
[17] Podevin P, Danlos A, Deligant M, Punov P, Clenci A and De La Bourdonnaye G 2018

Automotive compressor: effect of an electric throttle in the upstream circuit on the surge limit *MATEC Web Conf.* **234** 03006